





 Cite this: *RSC Adv.*, 2023, **13**, 9078

# Identification of peptide epitopes of the gp120 protein of HIV-1 capable of inducing cellular and humoral immunity†

 Jazmín García-Machorro,<sup>a</sup> Mara Gutiérrez-Sánchez,<sup>b</sup>  Diego Alexander Rojas-Ortega,<sup>b</sup> Martiniano Bello,<sup>c</sup> Sergio Andrade-Ochoa,<sup>de</sup> Sebastián Díaz-Hernández,<sup>c</sup> José Correa-Basurto <sup>\*c</sup> and Saúl Rojas-Hernández <sup>\*b</sup>

The Human Immunodeficiency Virus (HIV-1) causes Acquired Immunodeficiency Syndrome (AIDS) and a high percentage of deaths. Therefore, it is necessary to design vaccines against HIV-1 for the prevention of AIDS. Bioinformatic tools and theoretical algorithms allow us to understand the structural proteins of viruses to develop vaccines based on immunogenic peptides (epitopes). In this work, we identified the epitopes: P1, P2, P10, P27 and P30 from the gp120 protein of HIV-1. These peptides were administered intranasally alone or with cholera toxin (CT) to BALB/c mice. The population of CD4+, CD8+ T lymphocytes and B cells (CD19/CD138+, IgA+ and IgG+) from nasal-associated lymphoid tissue, nasal passages, cervical and inguinal nodes was determined by flow cytometry. In addition, anti-peptides IgG and IgA from serum, nasal and vaginal washings were measured by ELISA. The results show that peptides administered by i.n. can modulate the immune response of T and B lymphocyte populations, as well as IgA and IgG antibodies secretion in the different sites analyzed. In conclusion, bioinformatics tools help us to select peptides with physicochemical properties that allow the induction of the humoral and cellular responses that depend on the peptide sequence.

 Received 22nd December 2022  
 Accepted 12th March 2023

DOI: 10.1039/d2ra08160a

[rsc.li/rsc-advances](http://rsc.li/rsc-advances)

## Introduction

Acquired immunodeficiency syndrome (AIDS) in humans is caused by two retroviruses, the human immunodeficiency virus types 1 and 2 (HIV-1 and HIV-2).<sup>1</sup> They share a large number of similarities, including replication, transmission and clinical symptoms.<sup>2</sup> However, HIV-1 is responsible for most of the HIV infections worldwide causing 680 000 deaths in 2020 and 37.7 million people living with HIV worldwide.<sup>3</sup> It is important to mention that more than 80% of people with HIV-1 were infected

by mucosal exposure.<sup>4</sup> Due to the advance of the pandemic, the development of a vaccine against the virus has become a priority for scientists. However, the HIV genetic variability yields multiple genetic subtypes that make vaccine development difficult.<sup>5</sup> The most genetic variability occurs in the surface gp120 and gp41 envelope (Env) glycoproteins that mediate virus entry into the T lymphocytes of host cells.<sup>6,7</sup> Gp120 is very important for virus infection due to its initial recognition of some receptors such as DC-SIGN, heparan-sulfate proteoglycans and CD4 from T lymphocytes of the host.<sup>8</sup> One of the proposed mechanisms to prevent viral entry into host CD4+ cells and consequently avoid the infection, is through the blockage of gp120-CD4 complex formation.<sup>9</sup> In addition, the generation of neutralizing antibodies has attracted considerable attention, since they can compete with CD4 receptors, by joining the interface of both external and internal domains of the gp120 CD4 binding site (CD4bs).<sup>10</sup> Several studies have demonstrated that neutralizing antibodies are able to block the gp120 making this glycoprotein interesting for developing safe and effective vaccines for HIV.<sup>4,11</sup> However, to date, efforts to design and develop of HIV vaccines under traditional methods have not been successful.<sup>12</sup> At present, there are *in silico* strategies which allow the identification of possible epitopes (immunogenic peptides) from the linear sequence of proteins.<sup>13</sup> In addition, docking and molecular dynamics (MD) simulations are capable to discriminate among several epitopes based on differences in

<sup>a</sup>Laboratorio de Medicina de Conservación, Escuela Superior de Medicina, Instituto Politécnico. Plan de San Luis y Díaz Mirón s/n, Col. Casco de Santo Tomas, Delegación Miguel Hidalgo, C.P. 11340, Ciudad de México, Mexico

<sup>b</sup>Laboratorio de Inmunobiología Molecular y Celular, Sección de Estudios de Posgrado e Investigación, Escuela Superior de Medicina, Instituto Politécnico Nacional, México City, Mexico. E-mail: saulrohe@yahoo.com.mx

<sup>c</sup>Laboratorio de Diseño y Desarrollo de Nuevos Fármacos e Innovación Biotecnológica (Laboratory for the Design and Development of New Drugs and Biotechnological Innovation), Escuela Superior de Medicina, Instituto Politécnico Nacional. Plan de San Luis y Díaz Mirón s/n, Col. Casco de Santo Tomas, Delegación Miguel Hidalgo, C.P. 11340, Ciudad de México, Mexico. E-mail: corrjose@gmail.com

<sup>d</sup>Facultad de Ciencias Químicas, Universidad Autónoma de Chihuahua, Circuito Universitario S/N, 31125 Chihuahua, México

<sup>e</sup>Escuela Nacional de Ciencias Biológicas, Instituto Politécnico Nacional, Prolongación de Carpio y Plan de Ayala S/N, Colonia Santo Tomas, 11340 Ciudad de México, Mexico

† Electronic supplementary information (ESI) available. See DOI: <https://doi.org/10.1039/d2ra08160a>



affinity and peptide–protein complex stability on the major histocompatibility complex (MHC) both MHC-I and MHC-II.<sup>14,15</sup> In addition, the Quantitative Structure Activity-Relationship (QSAR) analysis allows obtaining the peptide properties that could aid to predict potential affinity between peptides on the MHC-I groove.<sup>16</sup> Rodríguez-Fonseca and collaborators evaluated *in silico* dendrimer-G4-PAMAM-peptide complexes using three-dimensional (3D) models of the gp120 from HIV-1 that were intranasally administered, either peptides alone or complexes to female BALB/c mice. They determined that the peptides were immunogenic at systemic and mucosal levels (nasal and vaginal), and G4-PAMAM dendrimer–peptide complexes had better IgG and IgA response in serum and nasal washes.<sup>17</sup>

Therefore, in order to have potential candidates for HIV-1 vaccines, in this work we focused to identify gp120 epitopes by combining bioinformatic epitope predictors, molecular docking, molecular dynamics (MD) simulations and QSAR studies. Once finished the *in silico* analyses, the peptides were synthesized and administered intranasally alone or with cholera toxin to BALB/c mice to assess their ability to induce CD4+ or CD8+ positive cells, plasma cells, IgG and IgA-specific antibodies.

## Materials and methods

### Theoretical procedure

#### Protein sequence search and multiple sequence analysis.

First, the gp-120 protein sequences indexed in the GenBank

database from HIV were searched and submitted to multiple sequence alignment using STRAP (Structure-based Sequence Alignment Program)<sup>18</sup> to identify the gp120-mutated and gp120-conserved regions to build a consensus sequence by using the muscle server: <https://www.ebi.ac.uk/Tools/msa/muscle/> (Fig. 1A).

**Homology modeling.** The Swiss-Model (<http://swissmodel.expasy.org/>) server was used for the automatic homology modeling<sup>19–21</sup> of the consensus sequence (Fig. 1A). The built 3D structures obtained were completed using the Modeller program (<http://www.salilab.org/modeller/>).<sup>22</sup> The 3D structure was subjected to analysis by the RAMPAGE Ramachandran (<http://eds.bmc.uu.se/ramachan.html>) server in order to validate the structure quality.<sup>23</sup>

**Prediction of immunogenic epitopes (MHC I, MHC II and B-cell epitopes).** The consensus sequence was submitted to ProPred (<https://webs.iitd.edu.in/raghava/propred/>, February 2023) and MHC2Pred, (<https://bio.tools/mhc2pred>, February 2023), servers for predicting the MHC-II epitopes. While the PreDep (<http://margalit.huji.ac.il/Teppred/mhc-bind/index.html>, February 2023), MCHPred (<http://www.ddg-pharmfac.net/mhcpred/MHCPred/>, February 2023), IEDB (<http://tools.immuneepitope.org/mhci/> February 2023) servers were used for predicting the MHC-I epitopes whereas the ElliPro (<http://tools.iedb.org/elliPro>, February 2023) server was used for the B-cell epitope predictions.

**Prediction proteasomal cleavages.** The proteasomal cleavages PaPROC ([www.paproc.de](http://www.paproc.de), February 2023) server was used

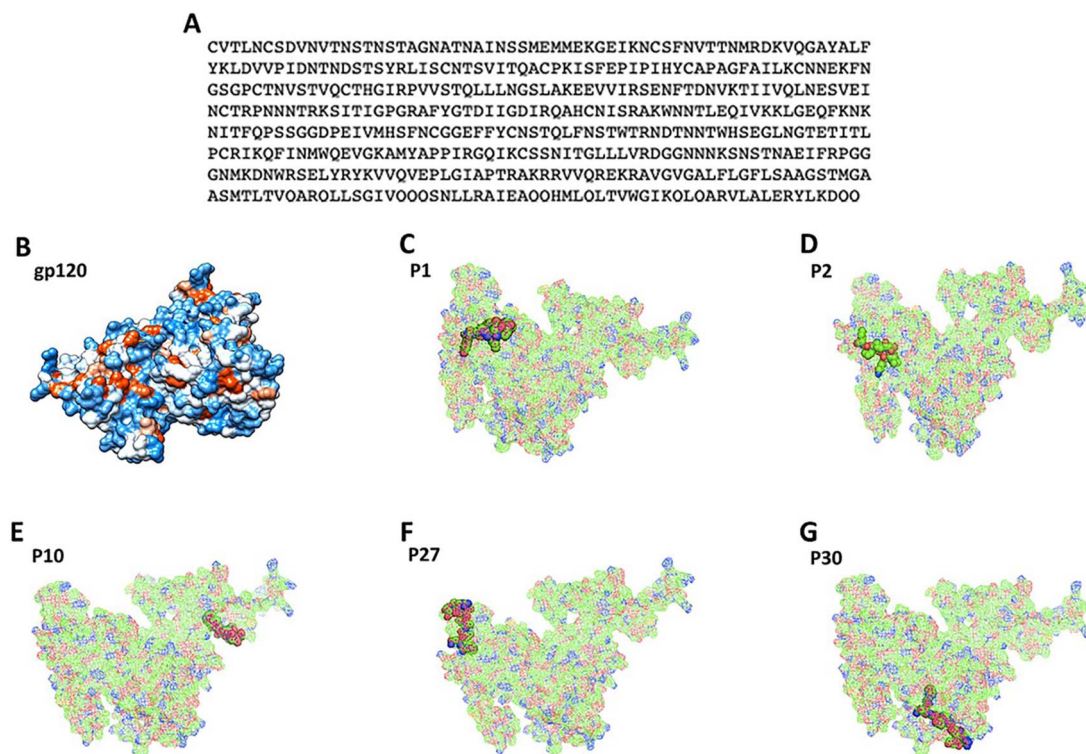


Fig. 1 Protein sequence and 3D modeled structure of the HIV-1 gp120. (A) Consensus sequence obtained by multiple alignments of 126 sequences of the HIV-1 gp120 protein. (B) 3D structure modeled from the consensus sequence of the HIV-1 gp120 protein. Immunogenic sequences exposed in the three-dimensional structures of the HIV-1 gp120 protein: (C) peptide P1, (D) peptide P2, (E) peptide P10, (F) peptide P27 and (G) peptide P30. All these peptides mentioned are marked with green, red and blue highlights.



Table 1 QSAR models for IC<sub>50</sub> HIV-I peptides in MHC-I<sup>a</sup>

QSAR models	
Model 1	$\log IC_{50} = -0.32477(E_{HOMO}) + 0.31845(Q_{tot}) - 0.023(AMR) - 0.17143(Alog P) - 2.31748$
Model 2	$\log IC_{50} = 0.34514(E_{HOMO}) - 5.08622(ICR) + 0.61229(Q_{tot}) - 0.23163(Hy) - 7.56378$
Model 3	$\log IC_{50} = -0.41182(I) + 4.77837(ICR) - 0.31823(Q_{tot}) - 0.13378(Alog P) - 11.18058$

<sup>a</sup>  $E_{HOMO}$  = energy of the HOMO orbital;  $Q_{tot}$  = total absolute charge;  $Alog P$  = Ghose–Crippen octanol–water partition coefficient; AMR = molar refractivity; ICR = radial centric information index; Hy = hydrophilic factor; I = ionization potential.

for degradation of the 30 most interesting predicted epitopes obtained by the servers previously mentioned.

**QSAR and DFT analysis.** The QSAR models were used to predict the interaction of the main peptides with the MHC-I following a procedure previously published.<sup>24</sup> The three main models are presented in Table 1.

**Molecular docking studies.** The selected epitopes were submitted to a docking study on MHC-I (PDB ID: 1HHH) and MHC-II (PDB ID: 1D5M) using the AutoDock4 software.<sup>25</sup>

The search space included  $\beta$ -folded chains and  $\alpha$ -helix chains of MHC following the previously published procedure.<sup>24</sup> A box  $70 \times 100 \times 90 \text{ \AA}$  with a grid spacing  $0.375 \text{ \AA}^3$  was generated. Docking parameters used were 100 runs, with 100 million energy evaluations for each test, and a population size of 100 individuals.<sup>26</sup> Peptide was treated as flexible. Results were analyzed using Autodock Tools software version 1.5.0 (<https://autodocksuite.scripps.edu/adt/>, February 2023) and figures were prepared with the Chimera software.<sup>27</sup>

**Multidocking approach of peptides on PAMAM-G4 dendrimer.** A methodology of multidocking approach (multimolecular coupling) was used following the procedure reported elsewhere.<sup>28</sup>

## Experimental procedures

**Peptides.** After *in silico* studies the best epitopes (P1, P2, P10, P27 and P30) were synthesized by SYN Peptide Co. with 99% purity grade chemically characterized by HPLC-ESI-MS.

**Preparation of peptides administered with cholera toxin.** Peptides were dissolved in Phosphates Buffer Solutions (PBS) ( $1.0 \text{ mg mL}^{-1}$ ) preparing stock solutions of  $150 \text{ \mu L}$ . For mice immunizations, peptides ( $30 \text{ \mu g}$ ) were administered alone or with  $2 \text{ \mu g}$  of CT (Sigma Aldrich®).

**Animals and immunizations.** All animals were handled in accordance with Mexican federal regulations for animal experimentation and care (NOM-062-ZOO-1999, Ministry of Agriculture, Mexico City, Mexico) and approved by the Institutional Animal Care and Use Committee (CICUAL-07/23-06-2017). In all experiments, 8–12 week-old female BALB/c mice were used.

The immunization schedule was carried out as was described by Rodríguez-Fonseca *et al.*, 2019,<sup>17</sup> briefly groups of 6 mice were immunized intranasal (i.n.), briefly mice were lightly anesthetized with ethyl ether, and subsequently applied doses with  $30 \text{ \mu g}$  of the peptide alone (P1, P2, P10, P27 and P30, respectively) or co-administered with CT, in total there were 3 immunizations on days 1, 7 and 14. The control mice received  $30 \text{ \mu L}$  of PBS.

**Sampling of immunized mice.** 24 h after the last immunization the serum, nasal and vaginal washes were collected. Then, all mice were slaughtered by cervical dislocation, and the following tissues were obtained for carrying out flow cytometry: lymphoid tissue associated with nose (NALT), nasal passages (NP), Cervical Nodes (CN) and Inguinal Nodes (IN). The cellular isolation from NALT, NP, CN and IN for flow cytometry assay was carried out as reported by Carrasco-Yepez *et al.*, 2018.<sup>29</sup> Serum, nasal and vaginal washes was stored at  $-20 \text{ }^\circ\text{C}$  until use.

**NALT isolation.** The lower jaw and tongue were removed from sacrificed mice. The palates were excised gripping behind incisor teeth with fine forceps and gently pulled to the molar teeth, using a scalpel to excise the tissue. Palates were placed into a 24 mm petri dish containing 3.0 mL of ice-cold RPMI-1640 medium supplemented with 5% heat-inactivated fetal bovine serum, 1% penicillin-streptomycin, 1% L-glutamine at pH 7.4, (Sigma Chemical Co., St Louis, MO, USA) and gently disaggregated to release cells. NALT cell suspensions from individual animals were pooled, and cells were resuspended in RPMI-1640 medium.

**Nasal passage isolation.** NP cells were isolated from the portion of the nasal cavity remaining after isolation of the NALT. The nasal cavity was rinsed with RPMI-1640 medium and transferred into a 15 mL conical centrifuge tube containing 3 mL of RPMI-1640 with  $440 \text{ U mL}^{-1}$  of type IV collagenase (Sigma Chemical Co.) and incubated horizontally at  $37 \text{ }^\circ\text{C}$  for 30 min in a shaker incubator at  $180 \text{ rpm min}^{-1}$ . After incubation, the released cells were centrifuged 10 min at 500 g and washed with RPMI-1640 medium. Cells were suspended in 4 mL of 40% Percoll (Pharmacia Fine Chemicals, Piscataway, NJ, USA) and overlaid onto 4 mL of 70% Percoll and centrifuged at 600 g for 25 min at room temperature. Cells from the interface were collected washed and resuspended in RPMI medium with 1% fetal calf serum.

**Nodes isolation.** CN and IN were identified and excised to be disaggregated with syringe needles to release cells and dispersed by syringing to obtain cell suspensions. All cell suspensions from each tissue were filtered through nylon mesh to remove tissue debris and washed twice with RPMI-1640 medium by centrifugation (500 g for 10 min at  $4 \text{ }^\circ\text{C}$ ). The cells were suspended in 4 mL of 40% Percoll (Pharmacia Fine Chemicals, Piscataway, NJ, USA) and overlaid onto 4 mL of 70% Percoll. Percoll gradients were centrifuged at 600 g per 25 min at  $4 \text{ }^\circ\text{C}$ . Cells from the interface were collected, washed and resuspended in RPMI medium supplemented with 1% fetal calf serum.





**Flow cytometry assays.** For the flow cytometry assay, all cell suspensions of each of NALT, PN, CN and IN were adjusted to  $1 \times 10^6$  cells per 1 mL in PBS. For analysis of the surface phenotype T cells were stained with CD4 (PerCP) and CD8a (APC) antibodies (BD biosciences). Cells were incubated for 30 min in the dark at room temperature. Subsequently, the cells were washed with PBS and fixed with 1% *p*-formaldehyde.

For the analysis of the percentage of B cells and IgG and IgA plasma cells, the antibodies (BD biosciences) were used: CD19 PE, CD138 APC and IgA FITC and IgG FITC. The cells were stained according to the BD Bioscience protocol for the detection of intracellular staining. The signal intensities were measured and analyzed by means of a FACSAria flow cytometer (Becton Dickinson) for the performance of relative fluorescence. 20 000 events were collected in the FSC/SSC point diagram.

**Quantification of IgG and IgA antibodies in immunized mice.** The levels of anti-peptide antibodies in the serum, nasal and vaginal washes samples were evaluated by the ELISA technique.<sup>17</sup> 96 well plates were coated with 10  $\mu$ g per well of the peptides (P1, P2, P10, P27 and P30, respectively) in 100  $\mu$ L of 0.1 M of NaHCO<sub>3</sub>/Na<sub>2</sub>CO<sub>3</sub> at pH 9.6 and incubated overnight at 4 °C, then washed several times with PBS-T. Plates were blocked with 100  $\mu$ L of 2% bovine serum albumin (BSA) in PBS-T and incubated 2 h at 37 °C. Plates were washed with PBS-T and incubated overnight at 4 °C with samples (100  $\mu$ L): sera in a 1 : 100 dilution and nasal and vaginal washings 1 : 2 dilution (100  $\mu$ L) for all groups. Subsequently, the plates were washed with PBS-T and incubated with 100  $\mu$ L goat anti-mouse IgG (Thermo scientific), anti-mouse IgA (Zymed Laboratories, San Francisco, CA) and anti-mouse IgM (Pierce, Rockford, IL) were added at a 1 : 6000, 1 : 500 and 1 : 3000 dilution respectively, the antibodies were incubated for 2 h at 37 °C. The plates were washed with PBS-T and the enzymatic reactions were started adding 100  $\mu$ L *o*-phenylenediamine 0.5 mg mL<sup>-1</sup> in phosphate-citrate buffer 50 mM, pH = 5.2 in the presence of H<sub>2</sub>O<sub>2</sub>. After 15 min, the reactions were stopped with 50  $\mu$ L of 2.5 M H<sub>2</sub>SO<sub>4</sub> and the absorbance at 492 nm (A492) was measured in a Multiscan Ascent (Thermo LabSystems) microplate reader.

**Statistical analysis.** For both flow cytometric and ELISAs techniques, data from six mice per group were reported as the mean  $\pm$  SD of three independent trials. In flow cytometry for background staining was controlled by labeled isotype controls (PharMingen) and never exceeded 1.0% of the cells. The results represent the percentage of positively stained cells in the total cell population that exceeds the background staining signal. Data were analyzed with Summit v4.3 software (Dako, Colorado Inc.). For the ELISA technique, in the figures, bars represent mean A490 values for antibody levels from each experimental group, along with standard deviations (SD) of three independent trials. The data obtained for flow cytometry and ELISA were statistically analyzed by means of a Unifance Analysis of Variance (ANOVA) and then a Tukey post hoc test using the PRISM computer program (GraphPad). A significance level with  $P < 0.05$ ,  $P < 0.01$  or  $P < 0.001$  was considered to establish that there was a significant difference between each group.

Table 2 Prediction results for the peptide–MHC I complex

Peptides		MCHPred		Predep	IEDB	
No.	Sequence	Position	IC <sub>50</sub>	Confidence	Energy	Percentile
P1	YRLISCNTS	76	23.77	0.78	-0.64	57.5
P2	FYKLDVVPI	59	0.55	1	-4.38	88
P3	VQLNESVEI	171	405.51	0.44	-2.63	77
P4	VVQVEPLGI	375	182.81	0.89	-4.09	15.5
P5	IKQLQARVL	460	17.5	1	-1.15	70
P6	IRPVVSTQL	139	70.47	1	-1.27	74.5
P7	IVQQQSNLL	435	7.33	1	-3.33	17.15
P8	IRQAHCNIS	209	20.99	0.89	1.16	71.5
P9	VITQACPPI	45	74.82	0.89	-4.05	72.5
P10	LGFLSAAGS	407	4.97	1	-3.98	86
P11	FFYCSTQL	264	32.36	1	-4.02	29.5
P12	LRAIEAQQH	443	181.55	0.89	0.49	62.5
P13	VPIDNTNDS	65	241.55	0.89	-0.67	48
P14	IRGQIKCSS	322	72.61	0.89	-0.33	82
P15	MLQLTVWGI	452	17.99	0.89	-4.96	16
P16	YKLDVVPI	60	231.21	0.89	-2.04	79
P17	LNGTETITL	291	671.43	0.89	-1.69	43.5
P18	YKVVQVEPL	373	34.91	1	-1.56	46.5
P19	FAILKCNNE	108	1.61	0.89	-0.79	58.5
P20	VVQREKRAV	392	192.31	0.78	-2.12	50.5
P21	LISCNTSV	78	17.46	1	-3.48	28.5
P22	LERYLKQQ	470	79.98	0.67	0.63	90.5
P23	LLSGIVQQQ	431	51.4	1	-1.73	59.5
P24	LSGIVQQQS	432	318.42	1	1.44	28.5
P25	LTVWGIKQL	445	127.94	0.89	-2.22	46.5
P26	VWGIKQLQA	457	260.62	1	-4.15	36.5
P27	FNVITNMRD	42	6.53	1	-2.19	68.5
P28	MTLTVQARQ	422	37.5	0.89	-1.72	30
P29	YAPPIRQI	318	6.32	1	-2.5	72.5
P30	FNSTWTRND	273	3.73	1	1.16	81

## Results

### Bioinformatic results

126 full sequences for gp120 protein of HIV-1 (from group M subtype B) were found at NCBI (ESI:† Fig. S1), being this subtype B the most predominant in the developed countries of the world, such as the United States and European countries,<sup>30</sup> and also, the most disseminated variant.<sup>31</sup> These protein sequences were submitted to multiple alignment sequence analysis obtaining a consensus sequence (Fig. 1A). This consensus sequence was used to build the 3D model (Fig. 1B and S2A†) which corresponds to report by Liu *et al.*<sup>32</sup> The Ramachandran analysis showed that 98% of the amino acids are in favorable regions (ESI:† Fig. S2B). Then, the consensus sequence was submitted to MHC-I epitope predictors (ProPred, MCHPred and IEDB) obtaining 30 peptides (Table 2).

Also, the consensus sequence submitted to MHC-II epitope predictors identified some epitopes predicted for MHC-I, ProPred: P1, P2 and P10 (ESI:† Fig. S3), MCH2Pred: P10 and IEDB: P2, P3, P13, P14, P29 (Table 3). In addition, ElliPRO identified some B-cell epitopes (Table 4) from the 3D structure.<sup>13</sup>

Finally, the PaPROC server allow us to discard some peptides that suffer degradation (ESI:† Table S1). As it is known,



Table 3 Prediction results for the peptide–MHC II complex<sup>a</sup>

Peptides			ProPred	MHC2Pred		IEDB
No.	Sequence	Position	Score	IC <sub>50</sub>	Confidence	Percentile
P1	YRLISCNTS	76	58.3	903.65	0.89	31.12
P2	FYKLDVVPI	59	57.2	WA	WA	89.62
P3	VQLNESVEI	171	34	3243.4	0.89	88.01
P4	VVQVEPLGI	375	30.83	1364.58	0.78	18.25
P5	IKQLQARVL	460	26.5	3715.35	0.89	4.16
P6	IRPVVSTQL	139	24	1174.9	1	28.42
P7	IVQQSNLL	435	36.67	4742.42	0.89	9.45
P8	IRQAHCNIS	209	39.77	1534.62	1	76.18
P9	VITQACPKI	85	32.83	2747.89	1	62.18
P10	LGFLSAAGS	407	54.09	9.68	1	2.91
P11	FFYCNSTQL	264	31.09	2249.05	0.89	15.4
P12	LRAIEAQQH	443	36.04	2971.67	0.89	32.89
P13	VPIDNTNDS	65	36.36	933.25	0.78	81.48
P14	IRGQIKCSS	322	33.71	2415.46	0.89	86.37
P15	MLQLTVWGI	452	31.33	4965.92	1	20.96
P16	YKLDVVPID	60	28.65	1224.62	1	76.36
P17	LNGTETITL	291	2.64	1279.38	0.89	72.08
P18	YKVVQVEPL	373	59.48	1364.58	0.78	13.37
P19	FAILKCNNE	108	32.58	WA	WA	54.81
P20	VVQREKRAV	392	19.28	WA	WA	65.58
P21	LISCNTSV	78	3.37	446.68	1	45.17
P22	LERYLKDQQ	470	1.63	2857.59	1	43.79
P23	LLSGIVQQQ	431	1.76	2259.44	1	28.79
P24	LSGIVQQQS	432	0.8	843.33	0.89	28.79
P25	LTVWGIKQL	445	1.86	847.23	0.89	32.72
P26	VWGIKQLQA	457	2.26	3715.35	0.89	32.72
P27	FNVTTNMRD	42	38.09	3126.08	0.89	64.64
P28	MTLTVQARQ	422	11.6	3435.58	1	35.38
P29	YAPPIRGQI	318	16.59	2857.59	0.89	86.37
P30	FNSTWTRND	273	22.34	WA	WA	76.14

<sup>a</sup> WA = without activity.

Table 4 Peptide conformational epitopes predicted as possible through the server ElliPro

No.	Peptides	Position	Score
P31	RQLLSGIVQ <sup>(P24)</sup> QQSPLLRAIEAQQHMLQLTVWGI <sup>(P15)</sup> KQL <sup>(P25)</sup> QARVLALERYLKDQQ <sup>(P22)</sup>	423	0.923
P32	FNVTTNMRD <sup>(P27)</sup> KVQAYALFYKLDVVPI <sup>(P2)</sup>	43	0.866
P33	GAYALFYKLDVVPI <sup>(P2)</sup> DNT	55	0.833
P34	LISCNTSV <sup>(P21)</sup>	79	0.825
P35	YLKDQQ <sup>(P22)</sup>	474	0.989
P36	RVLALER	467	0.981
P37	LTVWGIKQL <sup>(P25)</sup> QA	456	0.96
P38	QQSNLL	439	0.911
P39	LSGIVQ <sup>(P24)</sup>	433	0.878
P40	MTLTVQARQ <sup>(P28)</sup> L	423	0.821

antibodies must be able to reach the peptides on the 3D structure of gp120 selecting those peptides exposed on protein surface (Fig. 1C–G).

After all bioinformatic analyses described, five peptides were identified as promissory: P2 (FYKLDVVPI), P6 (IRPVVSTQL), P10 (LGFLSAAGS), P16 (YKLDVVPID) and P30 (FNSTWTRND). These peptides were submitted to QSAR using a mathematical prediction model.<sup>33</sup> Values of descriptors calculated for the five peptides exposed in the gp120 protein can be observed in ESI†

Table S2, while in Table 5 the prediction of IC<sub>50</sub> is found and the HOMO–LUMO densities (Fig. 2). The QSAR studies showed P2 as the most promissory according to the IC<sub>50</sub> values more favored according to model 1 and 3 (Table 5).

### Experimental results

**Peptides.** The immunogenicity of the peptides was evaluated in a murine model: peptide alone (P1, P2, P10, P27 and P30, respectively) or co-administrated with CT.



**Table 5** Prediction of the IC<sub>50</sub> (nM) on MHC-I of the exposed sequences of the gp120 protein using QSAR models

Peptides		Model 1		Model 2		Model 3	
No.	Sequence	log	IC <sub>50</sub>	log	IC <sub>50</sub>	log	IC <sub>50</sub>
P2	FYKLDVVPI	-1.06	0.09	0.60	4.03	-0.90	0.13
P6	IRPVVSTQL	0.52	3.34	2.39	243.27	1.57	36.79
P10	LGFLSAAGS	0.41	2.55	1.63	42.29	1.43	27.06
P16	YKLDVVPID	1.01	10.26	1.86	72.46	1.89	78.25
P30	FNSTWTRND	0.25	1.77	0.52	3.32	1.80	62.51

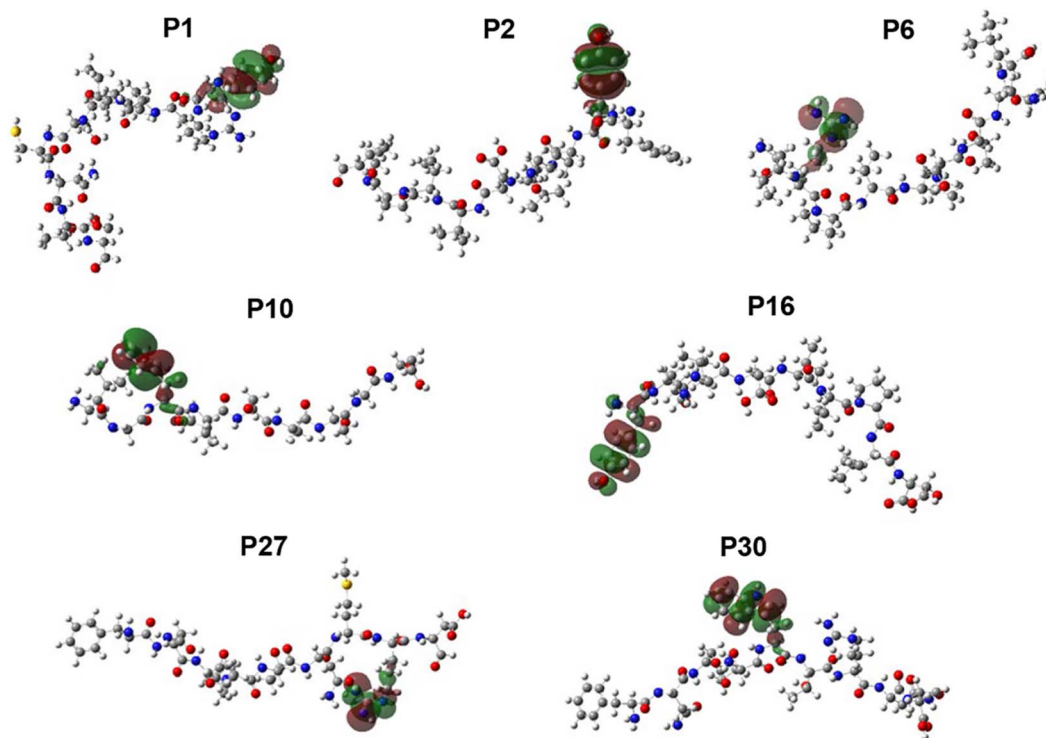
**Phenotypic CD4 and CD8 cells analyses.** The CD4+ and CD8+ cell phenotype was analyzed by flow cytometry in NALT, NP, CN and IN. The percentage of CD4+ T cells in the NALT increased significantly after administration of P2, P27, and P30 compared to the control group ( $P < 0.001$ ) (Fig. 3, Panel A). However, the percentages of CD4+ cells decreased significantly after administration with P1 and P10 concerning the control group ( $P < 0.001$ ) (Fig. 3, Panel A). P30 showed the highest significant increase compared to other peptides. Interestingly, this behavior is modified when peptides are administered with CT. The percentage of CD4+ T cells increased significantly compared to the control group where P2 had a higher significant percentage compared to the rest of the peptides. However, P2 co-administered with CT had no statistically significant difference with respect to P30.

Regarding CD8+ T lymphocytes, there was a significant increase ( $P < 0.001$ ) for all the peptides, except P1, which was

significantly lower than the control group ( $P < 0.001$ ). When the peptides were administered with CT, there was a significant increment in all the cases compared to the control group ( $P < 0.001$ ), being P27 which had the highest CD8+ T cell levels compared to the other peptides ( $P < 0.001$ ) (Fig. 3, Panel A).

Regarding to the lymphocyte phenotype in NP, the percentage of CD4+ lymphocytes was significantly higher with the peptides alone and peptides co-administered with CT compared to the control group ( $P < 0.001$ ). P2 showed a significantly higher increment compared to the rest of the peptides, either given alone or with CT ( $P < 0.001$ ). However, it was significantly higher co-administered with CT than alone ( $P < 0.01$ ). Like CD4+ cells, CD8+ T lymphocytes population showed a significant increment with peptides administered alone and peptides co-administered with CT compared to the control group ( $P < 0.001$ ), except for P1 treatment, which did not show a significant difference with the control group. Particularly, P2, P10, and P27 co-administrated with CT had a significantly higher increment compared with the other peptides ( $P < 0.001$ ) (Fig. 3, Panel B).

The percentage of CN lymphocytes show that CD4+ T lymphocytes decreased with the peptides alone or even with CT. Except, P30 alone or with CT which significantly increased the percentage of CD4+ compared to the control group ( $P < 0.05$ ). P30 alone was significantly higher than P30 co-administered with CT ( $P < 0.05$ ). Concerning CD8+ T lymphocytes, when P2, P10, and P27 were administered alone or with CT, they showed a significant increment in the cells percentage ( $P < 0.001$ ) compared to the control group (Fig. 3, Panel C).

**Fig. 2** Map of Highest Occupied Molecular Orbital (HOMO) of the peptides exposed in the three-dimensional structures of the HIV-1 gp120 protein.

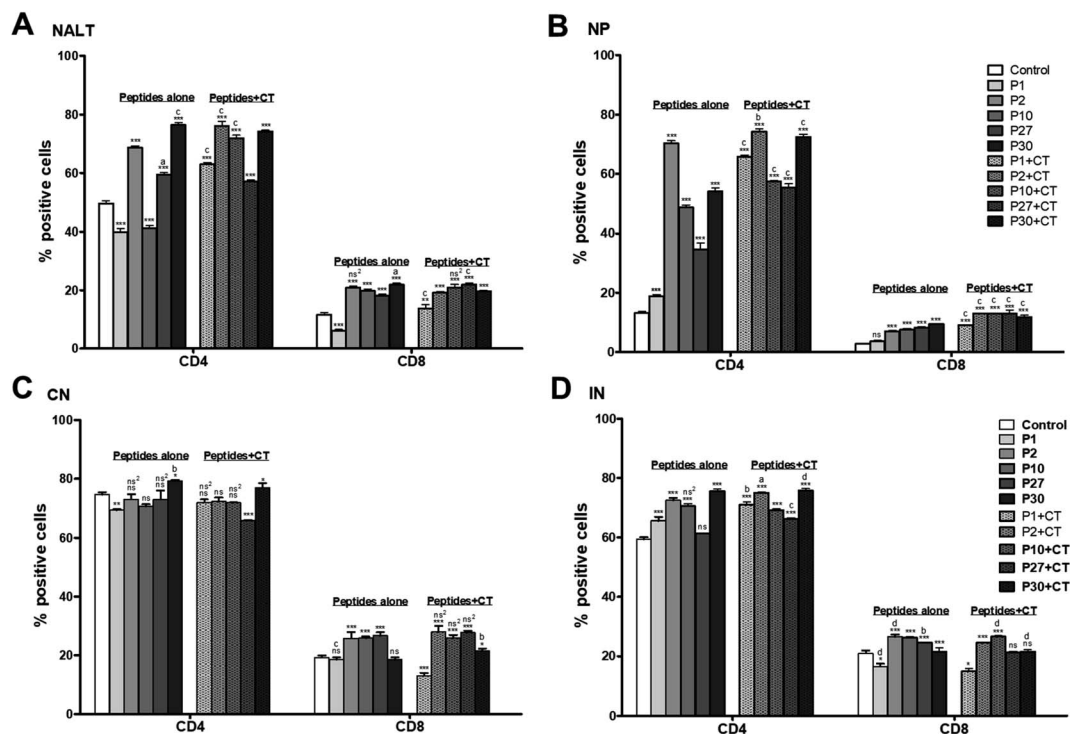


**Fig. 3** Phenotypic analysis of T CD4 and CD8+ cells from (A) NALT, (B) Nasal passages (NP), (C) Cervical Nodes (CN) and (D) Inguinal Nodes (IN). The peptides intranasally applied to each group were P1, P2, P10, P27 and P30 alone or with cholera toxin (CT). The control mice without treatment only received 30  $\mu$ L of PBS. Data represent mean percentages  $\pm$  SD from three independent experiments (using pooled cells of 6/group). The data obtained were statistically analyzed by means of a Unifance Analysis of Variance (ANOVA) and then a Tukey post hoc test. A significance level with  $P < 0.05$ ,  $P < 0.01$  or  $P < 0.001$  was considered to establish that there is a significant difference between each group. \* ( $P < 0.05$ ); \*\* ( $P < 0.01$ ); \*\*\* ( $P < 0.001$ ) and did not differ statistically significant (ns) compared to control. <sup>a</sup> ( $P < 0.05$ ), <sup>b</sup> ( $P < 0.01$ ), <sup>c</sup> ( $P < 0.001$ ) and did not differ statistically significant (ns<sup>2</sup>) compared to groups of peptides immunized alone or with CT.

The percentage for CD4+ T lymphocytes with P1, P2, P10, and P30 administered alone increased compared to the control group ( $P < 0.001$ ). P27 did not show a significant difference respect to the control. Instead, all the peptides co-administered with CT increased significantly compared to the control group ( $P < 0.001$ ). Emphasizing P30 alone or with CT which showed a significantly higher increment than other peptides. For CD8+ T lymphocytes, most of the peptides either alone or co-administered with CT promoted a significant increment compared to the control group ( $P < 0.001$ ), except for P27 with CT and P30 with CT which did not present a significant difference. While P2 alone or co-administrated with CT decreased compared to the control group ( $P < 0.05$ ) (Fig. 3, Panel D).

**B lymphocytes and plasma cells.** The percentage of activated positive B cells, as well as the percentage of plasma cells positive for IgA or IgG in cells purified from NALT, NP, CN, and IN were determined by flow cytometry.

The results obtained for NALT show a significant increase ( $P < 0.001$ ) for CD19/CD138 positive cells after immunization with the peptides alone (except P10) compared to the control group. When the peptides were co-administered with CT, most of the peptides showed a significant increment compared to the control group ( $P < 0.001$ ), only P1 with CT did not have a significant difference compared to the control group. However, P27 with CT was significantly higher than the other

peptides ( $P < 0.001$ ). Concerning IgA positive plasma cells, P1 alone significantly increased the percentage of cells compared to the control ( $P < 0.001$ ). Finding that P1 was significantly higher than the rest of the peptides ( $P < 0.001$ ). On the other hand, the administration of the peptides either alone or with CT significantly decreases the percentage of IgG positive plasma cells compared to the control group ( $P < 0.001$ ) (Fig. 4, Panel A).

Regarding to the peptide immunization in the NP, P1, P2, and P10 had a significant increment in the percentage of cells positive for CD19/CD138 ( $P < 0.001$ ) compared to the control group. P10 with CT was significantly higher than the other peptides ( $P < 0.001$ ). The analyses of IgA positive plasma cells showed that only P2 significantly increased the percentage of cells ( $P < 0.001$ ) compared to the control group. While peptides with CT in most cases increased the percentage of IgA compared to the control group ( $P < 0.001$ ), except for P30 with CT where no significant difference was found. P10 with CT was significantly higher than all the peptides ( $P < 0.001$ ). The immunization effect in the positive IgG cell percentage was completely different than it was for IgA cells where the intranasal administration with the peptides alone decreased the percentage of IgG cells in most cases ( $P < 0.001$ ). Only P27 showed a significant increment of IgG positive cells compared to the control and the other peptides ( $P < 0.001$ ) (Fig. 4, Panel B).





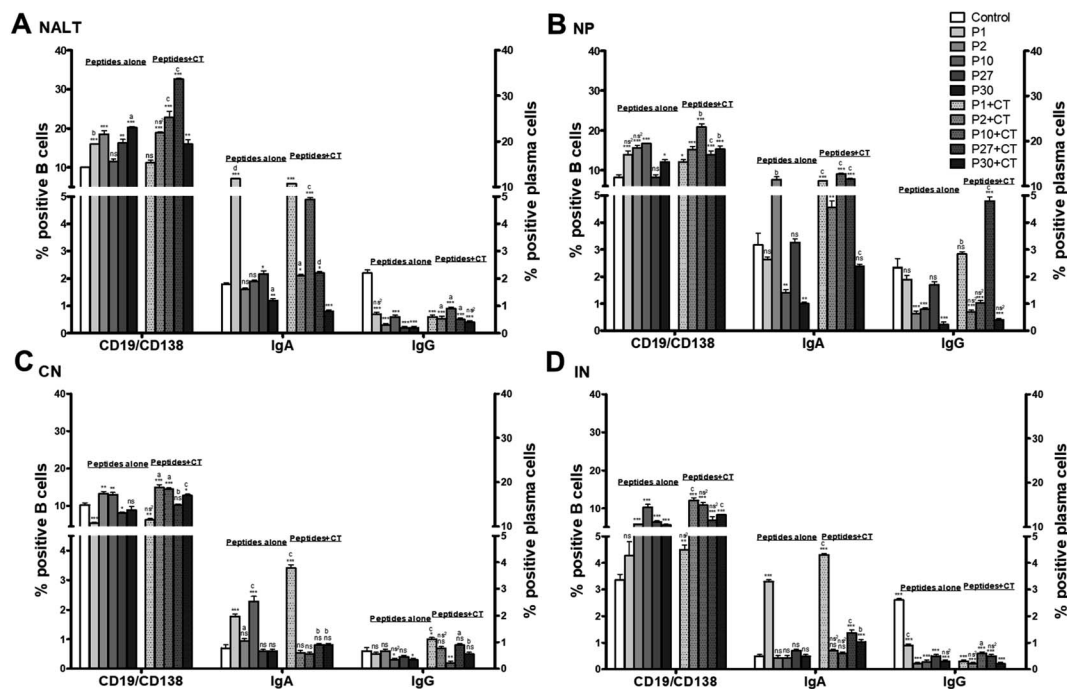


Fig. 4 Percentage of B lymphocytes expressing the activation markers CD19/CD138 and IgA and IgG antibodies forming cell from (A) NALT, (B) nasal passages (NP), (C) Cervical Nodes (CN) and (D) Inguinal Nodes (IN). The immunization intranasally each group were P1, P2, P10, P27 and P30 alone or with cholera toxin (CT). The control mice without treatment only received 30  $\mu$ L of PBS. Data represent mean percentages  $\pm$  SD from three independent experiments (using pooled cells of 6/group). The data obtained were statistically analyzed by means of a Unifance Analysis of Variance (ANOVA) and then a Tukey post hoc test. A significance level with  $P < 0.05$ ,  $P < 0.01$  or  $P < 0.001$  was considered to establish that there is a significant difference between each group. \* ( $P < 0.05$ ); \*\* ( $P < 0.01$ ); \*\*\* ( $P < 0.001$ ) and did not differ statistically significant (ns) compared to control. <sup>a</sup> ( $P < 0.05$ ), <sup>b</sup> ( $P < 0.01$ ), <sup>c</sup> ( $P < 0.001$ ) and did not differ statistically significant (ns<sup>2</sup>) compared to groups of peptides immunized alone or with CT.

The percentage of B lymphocytes in CN show that P2 and P10 significantly increased the cells ( $P < 0.01$ ). P30 did not show a significant difference, P1 ( $P < 0.001$ ), and P27 ( $P < 0.05$ ) showed a significant decrease compared with the control group. Interestingly, the administration of P2 and P10 with CT also significantly increased the percentage of CD19/CD138 positive cells compared to the control group ( $P < 0.001$ ) and compared to the other peptides ( $P < 0.05$ ). In the case of IgA-positive cells, the immunization with P1 or P10 significantly increased the percentage ( $P < 0.001$ ); while P2, P27, and P30 did not show a significant difference to the control group. When the peptides were co-administered with CT, only P1 showed a significant increase compared to the control group, and it was significantly higher than the other peptides ( $P < 0.001$ ). Regarding the percentage of plasma cells positive for IgG, the immunization with the peptides alone or with CT did not modify the percentage of cells, except for P1 co-administered with CT, which was the treatment that significantly increased the IgG-positive cells compared to the control and the other peptides ( $P < 0.05$ ) (Fig. 4, Panel C).

In addition, the results for the B lymphocytes in IN show that P1 did not have a significant difference to the control group, most of the peptides either alone or with CT were significantly higher than the control group ( $P < 0.001$ ), however, P1 with CT did not have a significant difference to the control group. P2 with CT was significantly higher than all the other peptides ( $P <$

0.001). Regarding the populations of plasma cells positive for IgA, only P1 induced a significant increase in the percentage of cells ( $P < 0.001$ ), while the other peptides did not induce significant differences. P1, P27, and P30 with CT significantly increased the percentage of cells compared with the control group. P1 with CT was significantly higher than all the other peptides either alone or with CT ( $P < 0.001$ ). The IgG-positive plasma cells populations significantly decreased with the administration of peptides alone or peptides with CT compared to the control group ( $P < 0.001$ ) (Fig. 4, Panel D).

**Flow cytometry dot-plots.** Representative dot-plots for selection criteria of cell populations for the P2 + CT from IN group are shown in ESI<sup>†</sup> Fig. S4, cells were gated based on size and granularity using FSC-A and SSC-A. Programs to determine region of lymphocytes were used; the same procedure was applied to all mice groups.

**Response of antibodies.** The IgG and IgA levels specific against the peptides from serum, nasal, and vaginal washes were determined by ELISA (Fig. 5). The nasal washes from immunized mice with peptides P27 or P30 had a significant increase in their anti-P27 and anti-p30 IgG levels respectively compared to the control group ( $P < 0.05$ ) (Fig. 5, Panel A). The coadministration of CT with P1, 27, and P30 significantly increased IgG compared to the control ( $P < 0.05$ ). P27 with CT was significantly higher than all the other peptides, either alone or with CT (Fig. 5, Panel A).





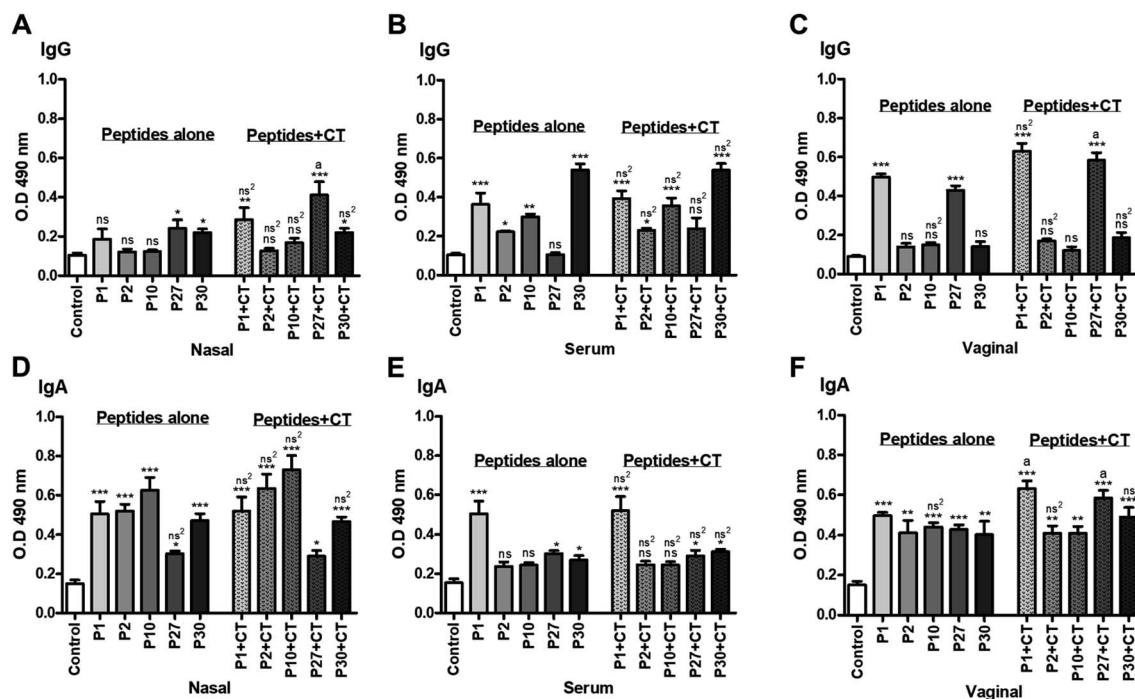


Fig. 5 Response of antibodies anti-peptide in serum, nasal washes and vaginal washes. Levels of IgG (items A–C) and IgA (items D–F) antibodies. The data obtained were statistically analyzed by means of a Unifance Analysis of Variance (ANOVA) and then a Tukey post hoc test. A significance level with  $P < 0.05$ ,  $P < 0.01$  or  $P < 0.001$  was considered to establish that there is a significant difference between each group. \* ( $P < 0.05$ ); \*\* ( $P < 0.01$ ); \*\*\* ( $P < 0.001$ ) and did not differ statistically significant (ns) compared to control. <sup>a</sup> ( $P < 0.05$ ), <sup>b</sup> ( $P < 0.01$ ), <sup>c</sup> ( $P < 0.001$ ) and did not differ statistically significant (ns<sup>2</sup>) compared to groups of peptides immunized alone or with CT.

The specific IgG in the serum shown that most of the peptides administered alone were capable to increment this antibody compared to the control where P1 and P30 had a difference of  $P < 0.001$ ; while P2 with  $P < 0.05$  and P10 with  $P < 0.01$ . In contrast, P27 did not present a significant difference to the control group. The administration of peptides with CT showed the same pattern as those administrated alone, finding that there was not a significant difference compared to the treatment with peptides alone (Fig. 5, Panel B).

Regarding to the specific IgG in vaginal washes, only P1 and P27 alone or co-administered with CT had a significant increase in anti-P1 and anti-P27 IgG levels compared to the control group ( $P < 0.001$ ), and such levels were significantly higher than the other peptides ( $P < 0.05$ ) (Fig. 5, Panel C).

The presence of specific IgA in nasal washes shown that peptides alone increase the specific IgA anti-peptides compared to the control group ( $P < 0.001$ ). Although immunization with P27 had a slight increase, this was still significant ( $P < 0.05$ ). IgA levels from immunized mice with peptides plus CT showed a similar pattern where a significant difference was found compared to the control mice. It is important to mention that in both cases, immunization with peptides alone as well as with CT had a similar IgA response, however, there are no significant differences between them (Fig. 5, Panel D).

About the specific IgA anti-peptides in serum, the P1 increased anti-P1 IgA levels compared with the control group ( $P < 0.001$ ). P27 and P30 immunization slightly increased IgA anti-P27 and anti-P30 compared to the control group ( $P < 0.05$ ). The

administration of P1 plus CT also showed that anti-P1 IgA levels was significantly increased compared to the control group ( $P < 0.001$ ). Although P27 + CT and P30 + CT slightly increase anti-P27, and anti-P30 IgA levels compared to the control group ( $P < 0.05$ ). Again, we can observe that no significant differences were found in the IgA response between the groups of mice immunized with the peptides alone or those co-administered with CT (Fig. 5, Panel E).

Finally, the specific IgA from vaginal washes show an increment in those mice immunized with P1, P10, P27 ( $P < 0.001$ ); P2 and P30 ( $P < 0.01$ ) compared to the control group. When P1, P27 and P30 ( $P < 0.001$ ), P2 and P10 ( $P < 0.01$ ) peptides were co-administered with CT, there was also a significant increment of IgA levels compared to the control group. Particularly, P1 with CT and P27 with CT were significantly higher than all the other peptides ( $P < 0.05$ ) (Fig. 5, Panel F).

## Discussion

The bioinformatics studies have become very important for the development of vaccines because the prediction of immunogenic peptides facilitates the design of friendly vaccines as has been performed for tuberculosis,<sup>34</sup> *Taenia solium*,<sup>35</sup> and even for cancer.<sup>36</sup> The peptide predictors reduce development costs and prevent unwanted responses produced with vaccines derived from attenuated pathogens, either alive or dead.<sup>37</sup> In this study there was used the consensus sequence (Fig. 1A) of full gp120 protein obtained after multiple alignment analyses.



The consensus sequence was used for building the 3D structure and predicting epitopes to identify antigens (Ag) capable to induce humoral and cellular responses for vaccination purposes. The peptide prediction for MHC-I and MHC-II binding regions yielded several lineal epitopes, and the non-lineal prediction was achieved by ElliProt identifying P2 into peptides P32 and P33 (Table 2). Moreover, the 3D structure visualization of gp120 showed five exposed predicted epitopes which can be recognized by antibodies (Fig. 1C–G).<sup>13</sup>

The QSAR model, which is based on predicting  $IC_{50}$  values, allows us to classify peptides that show affinity or not for the major histocompatibility complex (MHC), taking into account that lower  $IC_{50}$  has higher affinity.<sup>38</sup> We previously reported results for calculating the  $IC_{50}$  of HIV-1 immunogenic peptides.<sup>24</sup> In this work we use this model to calculate the  $IC_{50}$  of the peptides P2, P10, P27 and P30, obtaining outstanding  $IC_{50}$  values, however, the P2 was the better with a predicted  $IC_{50}$  of 0.09 mM and 0.13 mM for model 1 and model 3, respectively (Table 5), which could be explained as a consequence of its richness in electrons (Fig. 2), which favors its affinity to couple to MHC-I.<sup>24,38</sup> In addition, P2 and P10 have Tyr and Phe residues (Fig. 2) that could play an important role in the stabilization of macromolecular complexes due to their aromatic properties.<sup>39</sup> In addition, their spatial conformation of these peptides could suggest better recognition by antibodies generated through immunization.<sup>40</sup>

Peptides predicted and analyzed *in silico* (3D protein exposed,  $IC_{50}$  by QSAR) allow us to select the most promissory peptides (P1, P2, P10, P27 and P30) to be chemically synthesized and tested under experimental procedures. The target peptides were administered by intranasal immunization to female BALB/c mice, alone or with CT as adjuvant. Several studies have shown that intranasal immunization is effective in bringing together a local and systemic response. It is due to lymphocytes located at intranasal tissue can migrate by lymphatic system to other mucosal compartments reaching the respiratory tract, the gastric and genital tract,<sup>41</sup> where lymphocytes perform effector functions such as cytokine release and antibody secretion.<sup>42–44</sup> In addition, CT immunization as an adjuvant has been shown to modulate humoral responses, as well as modify populations of B and T lymphocytes, macrophages, and dendritic cells from various sites such as NALT, CN, NP, and spleen.<sup>29,45,46</sup>

These studies reinforce the results that we found since after intranasal immunization with the peptides (P1, P2, P10, P27, and P30) co-administered with CT increased the phenotype of CD4+ and CD8+ T lymphocytes in NALT, CN and IN compared to the control and immunized groups (Fig. 3).

It is important to note the presence of CD4+ or CD8+ T cells on these mentioned sites, may suggest that antigen-presenting cells travel to the distal mucosal compartments to generate a reservoir of cells from memory that can act when infection occurs as previously reported,<sup>47</sup> and furthermore, according to Wu *et al.*, 1997,<sup>48</sup> the nasal mucous membranes drain better in the cervical ganglia thanks to the permeability achieved with the use of CT as an adjuvant.

Once dendritic cells (DCs) captured the antigen from lumen antigen or lamina proper of nasal, they travel to the nearest

lymphoid nodule including the NALT and cervical ganglia, where they would be presenting the antigen to the T lymphocytes, thus initiating the inducing response.<sup>48</sup> In addition, the effector cells both T and B lymphocytes which express integrins ( $\alpha 4\beta 1$ ,  $\alpha 4\beta 7$ , *etc.*) as well as integrin receptors (CCR9, CCR10, *etc.*) on their surface that allow them to migrate to more distant nodules as the inguinal ganglia.<sup>49</sup>

The increase in the percentages of CD4+ and CD8+ T cells (particularly with P30 and P2 treatments) in NALT, CN and IN compared to the control group, suggests that the peptides are being captured by APC and processed for subsequent presentation to T lymphocytes. Then, the cell proliferation is carried out clonal by T cells, to have a favorable impact on the immune response, this could possibly have a positive effect on the challenge against virus infection, but more studies are needed to prove.

On the other hand, it is worth mentioning that the increase in B lymphocytes in the mice groups immunized with P2 and P10 in CN, as well as the increment in these B cells in all the mice groups immunized with each of the peptides (P1, P2, P10, P27 and P30) in IN, compared to the control group (Fig. 4 Sections C and D). These results suggests that Naive B lymphocytes were activated by the presence of the antigen and migrated to secondary lymphoid tissues. Activation may be mediated by dependent T antigens, a co-response with CD4 T lymphocytes, where in the germinal centers become plasma cells (PC) or memory cells, and there will also be a change immunoglobulin class.<sup>50</sup> PCs are terminally differentiated in plasmatic cells that provide protective immunity by producing antigen-specific antibodies.<sup>51</sup>

Therefore, the percentage of PC was analyzed, either positive for IgA or IgG. Populations of IgA positive cells show different behaviors according to the analyzed tissues (NALT, NP, CN and IN) and are the responses are depending of the groups immunized with the peptides alone or co-administered with CT (Fig. 4, items A–D). P1 + CT increases the percentage of positive cells in all sites analyzed, except in the nostrils compared to control. In the case of IgG positive PC, a decrease in the cellular percentage of all groups of immunized mice was obtained in most of the analyzed sites regarding control; except in the nostrils, where P27 + CT increased the percentage compared to control (Fig. 4, items A–D). These results allowed us to question whether IgA and IgG were soluble in the serum of immunized mice. Furthermore, several reports suggest that immunization of soluble proteins with CT stimulates Th1/Th2 responses.<sup>52</sup> Therefore, the presence of specific IgA and IgG antibodies against the designed peptides of HIV-1 gp120 in serum, nasal and vaginal washes was measured (Fig. 5, items A–F). In the case of IgG, there was observed that the administered peptides (P1, P2, P10, P27 and P30, respectively) did not show a significant difference with the control group in most cases (Fig. 5, items A–C); but when they were co-administered with CT, P1, and P27 result in an increased production of specific antibodies in nasal and vaginal lavages regarding control. While in serum, there was a significant increase in antibodies against the peptides being P30 with the best response either administered either alone or P30 + CT (Fig. 5B). Antibodies may participate in the



activation of cellular effector functions of the innate response, such as antibody-mediated cytotoxicity or phagocytosis; it is mediated by the recognition of antibodies bound to the antigen by Fcγ receptors present in immune cells such as macrophages, B cells, PC and neutrophils.<sup>53</sup> In the immune analysis of the RV144 HIV-1 vaccine efficacy trial conducted by Haynes *et al.*, 2012,<sup>54</sup> the estimated efficacy was significantly correlated with the binding of IgG antibodies to variable regions 1 and 2 (V1V2) of HIV-1 envelope proteins (Env) and the binding of IgA antibodies in plasma to Env, both mediated by the binding of antibodies against Fc receptors. This supports the idea that the FcR-binding Ig-HIV immunocomplex plays a critical role in protecting against HIV infection.

The tissues of the mucosa, such as the nasal or vaginal mucosa, contain IgA, although they can also contain IgG antibodies. The presence of IgG in the mucous membranes could be explained by the presence of the FcRn receptor, which mediates the transepithelial transport of IgG in various tissues, one of them the nasal mucosa.<sup>55</sup> The PCs in the lamina propria of the mucosa are mainly responsible to produce local IgA. Its epithelial transport is attributed to the presence of pIgR in the epithelial cells of the mucosa, which carries IgA from the basolateral region of the cells to the apical region.<sup>56</sup> The IgA and IgG titers in various tissues indicate that when the peptides were immunized alone or with the adjuvant, there was an elevation in the levels of specific antibodies (Fig. 5, items A-F). Antibodies present in mucous membranes and serum could have a neutralizing role for the HIV-1 virus and thus prevent infection. However, there are no long-term antibody protection findings in immunized patients.<sup>57</sup> Studies are needed to verify the protection that peptide-specific antibodies can provide against HIV infection. Furthermore, finding an increment of IgG in groups of immunized mice in serum suggests that a systemic response against peptides is being achieved, this is also important since these antibodies could act against the spread of the virus to the lymph nodes.

As previously was mentioned, HIV infection has been shown to cause dysregulation of the B lymphocyte population, significant memory cell loss, and therefore also decreased antibody production;<sup>58,59</sup> Therefore, it is a great result that the intranasal immunization with peptides from HIV-1 gp120 increase in IgA (in nasal and vaginal lavages) and IgG (in serum) (Fig. 5, items A-F). This suggests that the peptides can mount a local and systemic response when they are immunized intranasally and adjuvants with CT.

It is worth mentioning that the immune response induced by P2 does correspond with the results of the QSAR studies, which is a promising peptide to be a vaccine candidate (Table 5), however, we can say based on the experimental results that we found that all the peptides evaluated (P1, P2, P10, P27 and P30) are immunogenic, but this depended on the cell populations found of T and B lymphocytes, as well as IgA and IgG positive cells in the analyzed site, whether NALT, NP, CN and IN, as well as the levels of IgA and IgG antibodies in sera and nasal washes (Fig. 3-5). Therefore, the search and design of HIV-1 gp120 peptides using bioinformatics tools such as epitope prediction, docking and molecular dynamics simulations, as well as 3D

structure analysis docking, binding site prediction and simulation are tools of great importance in the design of promising vaccines under a guide of strategies that could elicit a protective immune response against HIV.

## Conclusions

Bioinformatics is useful in the prediction of epitopes with immunogenic potential; however, it is necessary to test in a biological system the induction of immune response (humoral and cellular response) since bioinformatic models are a mathematical approximation of some variables found in the organism, but do not consider all of them. In this work the information coincides for the peptides (P1, P2, P10, P27 and P30) studied that modify the response of both CD4 and CD8 lymphocytes as well as the response of IgA and IgG antibodies and this response was greater when the peptides were co-administered with CT. Another important aspect that is worth highlighting is that intranasal immunization is capable of inducing responses of both IgA and IgG antibodies, effector CD4 and CD8 T lymphocytes as well as cells positive for IgA and IgG locally (NALT and lamina propria) as well as in other mucosal compartments such as CN and IN. These strategies for the design of vaccines must be able not only to induce immunogenic responses but also to be immunoprotective; therefore, the use of bioinformatics tools is convenient for the choice of immunogenic epitopes, the immunization route, and the use of adjuvants.

## Abbreviations

AIDS:	Acquired immunodeficiency syndrome
APC:	Allophycocyanin
AuNPs:	Gold nanoparticles
CN:	Cervical nodes
CT:	Cholera toxin
FITC:	Fluorescein isoTioCyanat
HIV:	Human immunodeficiency virus
IN:	Inguinal nodes
mAbs:	Monoclonal antibodies
NALT:	Lymphoid tissue associated with nose
NP:	Nasal passages
PBS:	Phosphate-buffered saline
P1:	Peptide 1
P2:	Peptide 2
P10:	Peptide 10
P27:	Peptide 27
P30:	Peptide 30
PE:	Phycocerythrin
PerCP:	Peridinin-chlorophyll proteins

## Ethical approval

This study was conducted under licence according with the Mexican federal regulations for animal experimentation and



care (ESM, ESM.CICUAL-07/23-06-2017, NOM-062-ZOO-1999, Ministry of Agriculture, Mexico City, Mexico).

## Author contributions

Authors Saúl Rojas-Hernández, Jazmín García-Machorro and José Correa-Basurto conceived and planned the research. Author Mara Gutiérrez-Sánchez and Diego Alexander Rojas-Ortega carried out the experiments. Authors Saúl Rojas-Hernández, Jazmín García-Machorro, José Correa-Basurto and Mara Gutiérrez-Sánchez, steered the experiments. Authors Martiniano Bello, Sergio Andrade-Ochoa, Sebastián Díaz-Hernández carried out the bioinformatic studies. Authors Saúl Rojas-Hernández, Jazmín García-Machorro, José Correa-Basurto and Mara Gutiérrez-Sánchez analyzed data and conducted statistical analyses. Author Saúl Rojas-Hernández, Jazmín García-Machorro, José Correa-Basurto, Mara Gutiérrez-Sánchez and Diego Alexander Rojas-Ortega wrote the manuscript. All authors read and approved the manuscript.

## Conflicts of interest

The authors declare that they have no conflict of interest.

## Acknowledgements

The study was funded by the following grants: CIENCIA DE FRONTERA CONACYT 265230, PAPIIT-UNAM IN224519, IPN-SIP 20221248, CONACYT-CB-254600, CB-A1-S-21278, APN-782 and COFAA-SIP/IPN.

## References

- 1 P. M. Sharp and B. H. Hahn, *Cold Spring Harbor Perspect. Med.*, 2011, **1**, a006841.
- 2 S. Nyamweya, A. Hegedus, A. Jaye, S. Rowland-Jones, K. L. Flanagan and D. C. Macallan, *Rev. Med. Virol.*, 2013, **23**, 221–240.
- 3 T. Getaneh, A. Negesse, G. Dessie and M. Desta, *J. Clin. Tuberc. Other Mycobact. Dis.*, 2022, **27**, 100310.
- 4 M. S. Cohen, Y. Q. Chen, M. McCauley, T. Gamble, M. C. Hosseinipour, N. Kumarasamy, J. G. Hakim, J. Kumwenda, B. Grinsztejn, J. H. Pilotto, S. V. Godbole, S. Mehendale, S. Chariyalertsak, B. R. Santos, K. H. Mayer, I. F. Hoffman, S. H. Eshleman, E. Piwowar-Manning, L. Wang, J. Makhema, L. A. Mills, G. de Bruyn, I. Sanne, J. Eron, J. Gallant, D. Havlir, S. Swindells, H. Ribaud, V. Elharrar, D. Burns, T. E. Taha, K. Nielsen-Saines, D. Celentano, M. Essex and T. R. Fleming, *N. Engl. J. Med.*, 2011, **365**, 493–505.
- 5 J. R. Mascola and D. C. Montefiori, *Annu. Rev. Immunol.*, 2010, **28**, 413–444.
- 6 L. A. Araújo and S. E. Almeida, *Viruses*, 2013, **5**, 595–604.
- 7 V. Yoon, M. Fridkis-Hareli, S. Munisamy, J. Lee, D. Anastasiades and L. Stevceva, *Curr. Med. Chem.*, 2010, **17**, 741–749.
- 8 J. S. McLellan, M. Pancera, C. Carrico, J. Gorman, J.-P. Julien, R. Khayat, R. Louder, R. Pejchal, M. Sastry, K. Dai, S. O'Dell, N. Patel, S. Shahzad-ul-Hussan, Y. Yang, B. Zhang, T. Zhou, J. Zhu, J. C. Boyington, G.-Y. Chuang, D. Diwanji, I. Georgiev, Y. Do Kwon, D. Lee, M. K. Louder, S. Moquin, S. D. Schmidt, Z.-Y. Yang, M. Bonsignori, J. A. Crump, S. H. Kapiga, N. E. Sam, B. F. Haynes, D. R. Burton, W. C. Koff, L. M. Walker, S. Phogat, R. Wyatt, J. Orwenyo, L.-X. Wang, J. Arthos, C. A. Bewley, J. R. Mascola, G. J. Nabel, W. R. Schief, A. B. Ward, I. A. Wilson and P. D. Kwong, *Nature*, 2011, **480**, 336–343.
- 9 C. B. Wilen, J. C. Tilton and R. W. Doms, *Cold Spring Harbor Perspect. Med.*, 2012, **2**, 1–13.
- 10 S. Zolla-Pazner, *Nat. Rev. Immunol.*, 2004, **4**, 199–210.
- 11 J. P. Moore, P. W. Parren and D. R. Burton, *J. Virol.*, 2001, **75**, 5721–5729.
- 12 B. F. Haynes, *Curr. Opin. Immunol.*, 2015, **35**, 39–47.
- 13 J. Ponomarenko, H. H. Bui, W. Li, N. Füsseder, P. E. Bourne, A. Sette and B. Peters, *BMC Bioinf.*, 2008, **9**, 514.
- 14 C. Cárdenas, A. Bidon-Chanal, P. Conejeros, G. Arenas, S. Marshall and F. J. Luque, *J. Comput.-Aided Mol. Des.*, 2010, **24**, 1035–1051.
- 15 J. M. Khan and S. Ranganathan, *Immunome Res.*, 2010, **6**(1), S2.
- 16 D. Flower, H. McSparron, M. Blythe, C. Zygouri, D. Taylor, P. Guan, S. Wan, P. Coveney, V. Walshe, P. Borrow and I. Doytchinova, *Novartis Found. Symp.*, 2003, **254**, 102–120.
- 17 R. A. Rodríguez-Fonseca, M. Bello, M. de Los Muñoz-Fernández, J. Luis Jiménez, S. Rojas-Hernández, M. J. Frago-Vázquez, M. Gutiérrez-Sánchez, J. Rodríguez, N. Cayetano-Castro, R. Borja-Urby, O. Rodríguez-Cortés, J. García-Machorro and J. Correa-Basurto, *Colloids Surf., B*, 2019, **177**, 77–93.
- 18 C. Gille and C. Frommel, *Bioinformatics*, 2001, **17**, 377–378.
- 19 K. Arnold, L. Bordoli, J. Kopp and T. Schwede, *Bioinformatics*, 2006, **22**, 195–201.
- 20 F. Kiefer, K. Arnold, M. Kunzli, L. Bordoli and T. Schwede, *Nucleic Acids Res.*, 2009, **37**, D387–D392.
- 21 M. C. Peitsch, *Bio/Technology*, 1995, **13**, 658–660.
- 22 A. Sali and T. L. Blundell, *J. Mol. Biol.*, 1993, **234**, 779–815.
- 23 S. C. Lovell, I. W. Davis, W. B. Arendall 3, P. I. de Bakker, J. M. Word, M. G. Prisant, J. S. Richardson and D. C. Richardson, *Proteins*, 2003, **50**, 437–450.
- 24 S. Andrade-Ochoa, J. García-Machorro, M. Bello, L. M. Rodríguez-Valdez, C. A. Flores-Sandoval and J. Correa-Basurto, *J. Biomol. Struct. Dyn.*, 2018, **36**, 2312–2330.
- 25 G. M. Morris, R. Huey, W. Lindstrom, M. F. Sanner, R. K. Belew, D. S. Goodsell and A. J. Olson, *J. Comput. Chem.*, 2009, **30**, 2785–2791.
- 26 P. K. Loyola, R. Campos-Rodríguez, M. Bello, S. Rojas-Hernández, M. Zimic, M. Quiliano, V. Briz, M. A. Muñoz-Fernández, L. Tolentino-Lopez and J. Correa-Basurto, *Immunol. Res.*, 2013, **56**, 44–60.
- 27 E. F. Pettersen, T. D. Goddard, C. C. Huang, G. S. Couch, D. M. Greenblatt, E. C. Meng and T. E. Ferrin, *J. Comput. Chem.*, 2004, **25**, 1605–1612.





- 28 R. G. Bellini, A. P. Guimaraes, M. A. Pacheco, D. M. Dias, V. R. Furtado, R. B. de Alencastro and B. A. Horta, *J. Mol. Graphics Modell.*, 2015, **60**, 34–42.
- 29 M. M. Carrasco-Yepey, R. Campos-Rodríguez, A. A. Reséndiz-Albor, C. Peña-Juárez, A. Contis-Montes de Oca, I. M. Arciniega-Martínez, P. Bonilla-Lemus and S. Rojas-Hernandez, *Parasite Immunol.*, 2018, **40**, 1–10.
- 30 M. Santerre, Y. Wang, S. Arjona, C. Allen and B. E. Sawaya, *AIDS Rev.*, 2019, **21**, 76–83.
- 31 D. M. Junqueira and S. E. Almeida, *Virology*, 2016, **495**, 173–184.
- 32 S. Q. Liu, S. X. Liu and Y. X. Fu, *J. Mol. Model.*, 2008, **14**, 857–870.
- 33 M. A. Toropova, A. M. Veselinović, J. B. Veselinović, D. B. Stojanović and A. A. Toropov, *Comput. Biol. Chem.*, 2015, **59**, 126–130.
- 34 D. Ortega-Tirado, E. I. Niño-Padilla, A. A. Arvizu-Flores, C. Velazquez, C. Espitia, C. J. Serrano, J. A. Enciso-Moreno, A. Sumoza-Toledo and A. Garibay-Escobar, *Mol. Immunol.*, 2020, **125**, 123–130.
- 35 M. Zimic, A. H. Gutiérrez, R. H. Gilman, C. López, M. Quiliano, W. Evangelista, A. Gonzales, H. H. García and P. Sheen, *Bioinformation*, 2011, **6**, 271–274.
- 36 J. Liu, M. Fu, M. Wang, D. Wan, Y. Wei and X. Wei, *J. Hematol. Oncol.*, 2022, **15**, 28.
- 37 R. J. Malonis, J. R. Lai and O. Vergnolle, *Chem. Rev.*, 2020, **120**, 3210–3229.
- 38 S. Corbet, H. V. Nielsen, L. Vinner, S. Lauemoller, D. Therrien, S. Tang, G. Kronborg, L. Mathiesen, P. Chaplin, S. Brunak, S. Buus and A. Fomsgaard, *J. Gen. Virol.*, 2003, **84**, 2409–2421.
- 39 M. Jirásek, M. Rickhaus, L. Tejerina and H. L. Anderson, *J. Am. Chem. Soc.*, 2021, **143**, 2403–2412.
- 40 G. L. Ramírez-Salinas, J. García-Machorro, S. Rojas-Hernández, R. Campos-Rodríguez, A. C. de Oca, M. M. Gomez, R. Luciano, M. Zimic and J. Correa-Basurto, *Arch. Virol.*, 2020, **165**, 891–911.
- 41 S. Rojas-Hernández, M. A. Rodríguez-Monroy, R. López-Revilla, A. A. Reséndiz-Albor and L. Moreno-Fierros, *Infect. Immun.*, 2004, **72**, 4368–4375.
- 42 M. Carrasco-Yepey, R. Campos-Rodríguez, I. Lopez-Reyes, P. Bonilla-Lemus, A. Y. Rodríguez-Cortés, A. Contis-Montes de Oca, A. Jarillo-Luna, A. Miliar-García and S. Rojas-Hernandez, *Exp. Parasitol.*, 2014, **145**, S84–S92.
- 43 A. Jarillo-Luna, L. Moreno-Fierros, R. Campos-Rodríguez, M. A. Rodríguez-Monroy, E. Lara-Padilla and S. Rojas-Hernández, *Parasite Immunol.*, 2008, **30**, 31–38.
- 44 N. Lycke, *Nat. Rev. Immunol.*, 2012, **12**, 592–605.
- 45 R. F. Rolando Alberto, B. Martiniano, R. H. Saúl, G. M. Jazmín, G. S. Mara, E. P. Alan Rubén, F. V. Manuel Jonathan, M. M. Juan Vicente and C. B. José, *RSC Adv.*, 2020, **10**, 20414–20426.
- 46 I. Jabbal-Gill, *J. Drug Targeting*, 2010, **18**, 771–786.
- 47 H. Y. Wu, E. B. Nikolova, K. W. Beagley and M. W. Russell, *Immunology*, 1996, **88**, 493–500.
- 48 H. Y. Wu, E. B. Nikolova, K. W. Beagley, J. H. Eldridge and M. W. Russell, *Infect. Immun.*, 1997, **65**, 227–235.
- 49 E. J. Kunkel and E. C. Butcher, *Immunity*, 2002, **16**, 1–4.
- 50 J. R. Mora and U. H. von Andrian, *Mucosal Immunol.*, 2008, **1**, 96–109.
- 51 X. Wang, G. L. Hao, B. Y. Wang, C. C. Gao, Y. X. Wang, L. S. Li and J. D. Xu, *Cell Biosci.*, 2019, **9**, 26.
- 52 H. P. Jones, L. M. Hodge, K. Fujihashi, H. Kiyono, J. R. McGhee and J. W. Simecka, *J. Immunol.*, 2001, **167**, 4518–4526.
- 53 F. Nimmerjahn and J. V. Ravetch, *Nat. Rev. Immunol.*, 2008, **8**, 34–47.
- 54 B. F. Haynes, P. B. Gilbert, M. J. McElrath, S. Zolla-Pazner, G. D. Tomaras, S. M. Alam, D. T. Evans, D. C. Montefiori, C. Karnasuta, R. Sutthent, H. X. Liao, A. L. DeVico, G. K. Lewis, C. Williams, A. Pinter, Y. Fong, H. Janes, A. DeCamp, Y. Huang, M. Rao, E. Billings, N. Karasavvas, M. L. Robb, V. Ngauy, M. S. de Souza, R. Paris, G. Ferrari, R. T. Bailer, K. A. Soderberg, C. Andrews, P. W. Berman, N. Frahm, S. C. De Rosa, M. D. Alpert, N. L. Yates, X. Shen, R. A. Koup, P. Pitisuttithum, J. Kaewkungwal, S. Nitayaphan, S. Rerks-Ngarm, N. L. Michael and J. H. Kim, *N. Engl. J. Med.*, 2012, **366**, 1275–1286.
- 55 S. Heidl, I. Ellinger, V. Niederberger, E. E. Walzl and R. Fuchs, *Protoplasma*, 2016, **253**, 1557–1564.
- 56 R. E. Horton and G. Vidarsson, *Front. Immunol.*, 2013, **4**, 200.
- 57 H. Billings, B. D. Wines, W. B. Dyer, R. J. Center, H. M. Trist, S. J. Kent and P. M. Hogarth, *AIDS Res. Hum. Retroviruses*, 2019, **35**, 842–852.
- 58 A. De Milito, C. Mörch, A. Sönnnerborg and F. Chiodi, *AIDS*, 2001, **15**, 957–964.
- 59 H. Longwe, S. Gordon, R. Malamba and N. French, *BMC Infect. Dis.*, 2010, **10**, 280.

